V.O. Kotsyubynsky[1], V.M. Boychuk[1], R.I. Zapukhlyak[1], M.A. Hodlevskyi[1],
I.M. Budzulyak[1], A.I. Kachmar[2], M.A. Hodlevska[1], L.V. Turovska[3]

Electrophysical and Morphological Properties of a Hydrothermally Synthesized CuFe₂O₄ and CuFe₂O₄ / Reduced Graphene Oxide Composite

[1]Vasyl Stefanyk Precarpathian National University, Ivano-Frankivsk, Ukraine. kotsuybynsky@gmail.com
[2]Poznan University of Technology, Poland, andrij.nj@gmail.com
[3]Ivano-Frankivsk National Medical University, Ivano-Frankivsk, Ukraine, lturovska@gmail.com

The aim of this paper is to compare the structural, morphological and electrical properties of the CuFe₂O₄ and CuFe₂O₄ / reduced graphene oxide composite. XRD and Mossbauer studies have shown that joint hydrothermal synthesis of cubic copper ferrite and reduction of graphene oxide leads to a decrease in ferrite particles from 14 to 8 nm. Based on the impedance spectroscopy data, a model of the obtained composite material has been prepared as a system consisting of contacting spinel particles covered with rGO clusters and separated by porous rGO. For CuFe₂O₄ / rGO composite material, the predominance of hopping charge transfer mechanisms has been shown, and the activation energies of electrical conductivity of grains and grain boundaries have been calculated.

Keywords: copper ferrite, reduced graphene oxide, Mossbauer spectroscopy, pore size distribution, electrical conductivity.

Introduction

Transition metal oxides with a spinel structure are promising pseudocapacitive electrode materials for hybrid supercapacitors due to their high electrochemical performance in aqueous electrolytes combined with long-term stability and low cost [1]. Some of them, primarily CoFe₂O₄ [2], MnFe₂O₄ [3] and NiFe₂O₄ [4], have already been successfully tested as electrode materials for super-capacitors. Other systems, such as CuFe₂O₄, are currently being studied to find optimal synthesis conditions that would make it possible to obtain an active material with balanced structural, morphological and electrophysical properties. A hybrid electrochemical capacitor (HEC) combines a battery-type electrode with charge storage via a surface redox reaction and another carbon-based electrode, where the electrostatic charge storage mechanism involves the formation of an electric double layer at the electrode / electrolyte interface. An increase in the specific power and energy of modern HEC requires the optimization of all components of the electrochemical system – an oxide cathode, an eco-friendly aqueous electrolyte and a carbon-based anode. The main drawback of spinel electrodes is the correspondingly low electronic conductivity, which limits the rate of the surface Faradaic reaction. The formation of carbon nanocomposites makes it possible to improve the electrochemical performance of the cathode due to the synergistic effects of a highly developed porous structure in combination with good electrical conductivity. This approach improves the charge exchange between transition metal ions on the surface of oxide nanoparticles and the electrolyte. Reduced graphene oxide (rGO) is a technologically low-cost version of graphene and has important energy storage properties due to its high specific surface area and good electronic conductivity combined with pseudocapacitive activity [5].

It is obvious that the stage of synthesis is extremely important for obtaining nanostructured composite electrode materials with balanced properties. The main advantage of hydrothermal synthesis of spinel oxide / rGO systems is the ability to control morphology and electrical conductivity at the stage of joint nucleation and growth of both components of the nanocomposite. This work presents the results of the hydrothermal synthesis of nanostructured $CuFe_2O_4$ and $CuFe_2O_4$ / rGO composites. The main difference between this study and the previous one [6] lies in a modified synthesis protocol, which assumes the use of colloidal graphene oxide obtained by an original approach in the synthesis [7]

I. Experimental details

Synthesis of materials

Nanostructured $CuFe_2O_4$ as well as $CuFe_2O_4$ / rGO composites were synthesized by a one-step hydrothermal technique. In order to prepare copper ferrite, NaOH (0.01 M) aqueous solution was added dropwise with vigorous stirring to a mixture of $Fe_2(SO_4)_3 \cdot (0.1$ M) and $CuSO_4 \cdot 5H_2O$ (0.1 M). The resulting colloidal solution was ultrasonicated for 1 h to obtain a sparse suspension, transferred to a Teflon-lined stainless steel autoclave and kept at 150 °C for 10 h. After cooling, the obtained precipitate was collected, alternately washed with deionized water and ethanol, and then dried at 80 °C. Aqueous colloidal GO was obtained by the modified Tour method [7] and used as an additive in the synthesis of the $CuFe_2O_4$ / rGO composite material. Hydrothermal treatment of the colloidal solution of GO was carried out under the same experimental conditions as the estimated reduction process. The prepared black fine powder after washing and drying was marked as rGO sample. The estimated mass ratio between spinel and rGO phases in the composite was close to 1:1.

Characteristics of materials

The structural characteristics of the obtained powders were carried out using the XRD (DRON-3M powder diffractometer, Cu Kα radiation). The average size of the coherent scattering domains (CSD) was calculated using Scherrer equation. The morphological properties were investigated by the low-temperature nitrogen absorption / desorption porosimetry (Quantachrome Autosorb Nova 2200e device). The chemical composition of the obtained materials was investigated by X-ray fluorescence analysis (Expert 3L device). The Mössbauer spectra were measured in transmission geometry using a MS-1104Em spectrometer in the constant acceleration mode and a $^{57}Co(Cr)$ γ-ray source. The velocity scale was calibrated relative to α-Fe. The Mosswin 3.0 software was used to quantitatively estimate the spectral parameter. The frequency dependence of the electrical conductivity was investigated by impedance spectroscopy (Autolab PGSTAT 12 / FRA-2 device) in the frequency range of 0.01 - 100 kHz and in the temperature range of 25 - 200 °C. The electrical conductivity was measured for cylindrical samples prepared by pressing at 20 kN.
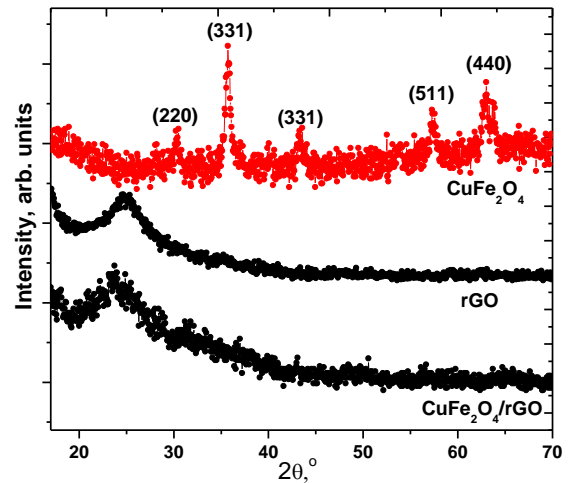

Fig. 1. XRD patterns of hydrothermally synthesized $CuFe_2O_4$ and $CuFe_2O_4$ / rGO samples.

II. Results and discussion

Fig. 1 shows XRD patterns of $CuFe_2O_4$, rGO and $CuFe_2O_4$ / rGO powders. The XRD pattern of the $CuFe_2O_4$ sample matches with the JCPDS 77-0010 and can be assigned to a face-centered cubic spinel, space group Fd-3m. The observed s peaks at 2θ = 30.0, 35.5, 43.3, 57.3, and 62.8° are attributed to the (220), (311), (400), (511), and (440) crystal planes of the cubic spinel structure.

The average size D of CSD of the $CuFe_2O_4$ sample was calculated using the Scherrer equation: $D = K\lambda / \beta\cos\theta$, where $\lambda = 0.15406$ nm is the X-ray wavelength, $K = 0.89$ is a constant that depends on the crystal shape, β is FWHM of the most intensive (311) reflex measured using the best Lorentzian fit, θ is the Bragg angle. The estimated average size of CSD of pure phase $CuFe_2O_4$ ferrite is about 14 nm.

The broad peak in the range of about $2\theta = 20$-$30°$, observed in the XRD patterns of the rGO and $CuFe_2O_4$ / rGO samples, corresponds to the (002) reflexes of the structure of reduced graphene oxide [6] (Fig.1, a). The XRD profiles were fitted with a Gaussian function, which allows the most probable values of $d_{(002)}$ and D of rGO crystallites to be calculated for these two samples. The rGO material is composed of crystallites with an average interplanar distance $d_{(002)}$ of 0.356 nm and a thickness D of 2.52 nm (linear size in the direction perpendicular to the basal (002) plane), consisting of approximately 8 graphene layers. The obtained $d_{(002)}$ value is close to the (002) interplanal distance for bulk graphite (0.33 nm), which indicates a high degree of reduction due to the removal of surface oxygen-containing groups and restoration of the crystal lattice [8]. The fraction of rGO crystallites in the powder of the $CuFe_2O_4$ / rGO composite has an average thickness of about 2.20 nm and consists of about 7 graphene layers ($d_{(002)} = 0.365$ nm). The observed structural changes in the rGO fraction of the composite structure as compared to pure rGO correspond to an increase in the material
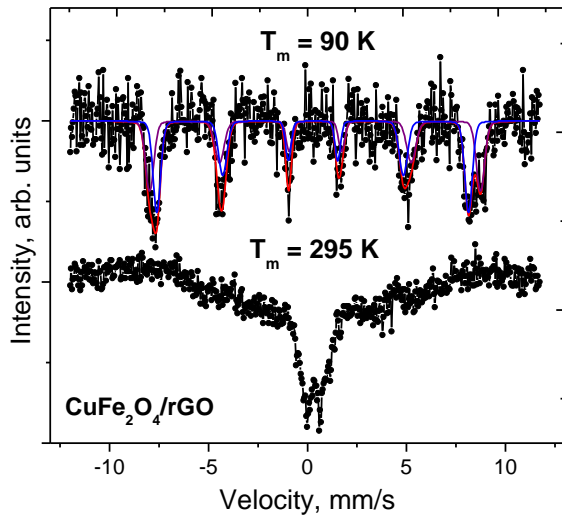
Fig. 2. Mössbauer spectra of $CuFe_2O_4/rGO$ composite materials measured at 295 and 90 K.

dispersion of both spinel and carbon components. A decrease in the average particle size of the spinel phase in $CuFe_2O_4/rGO$ leads to the absence of reflexes in XRD pattern.

Low temperature Mössbauer studies provide independent information on the structural ordering of ultrafine materials with CSD sizes, which make it impossible to obtain a diffraction pattern without using synchrotron radiation sources. The Mössbauer spectra of the $CuFe_2O_4/rGO$ sample measured at measurement temperatures of 295 and 90 K, respectively, are shown in Fig. 2. The spectra at room temperature are a superposition of the components of doublet and very broad sextet. The first corresponds to γ-quantum resonance absorption by nuclei of tetrahedral coordinated ions of high-spin Fe^{3+} in the paramagnetic state. The formation of the doublet component is the result of size effects and superparamagnetism phenomena [9]. The obtained materials can be represented as systems of ferrite nanoparticles with uniaxial magnetic anisotropy. Under these conditions, the monodomain state of ferrimagnetic clusters becomes predominant, which causes fluctuations in the magnetic moment of the particle between the directions of easy magnetization axes. The relaxation time τ_0 can be calculated as [10]

$$\tau_r = \tau_0 \exp\left(\frac{KV}{kT}\right),$$ where $\tau_0 \approx 10^{-9}$ s, V is particle

volume, K is anisotropy constant, T is temperature. When the relaxation time becomes shorter than the lifetime of the excited state of Co^{57} (registration time), the particle will be registered as paramagnetic. Fluctuations cause broadening of the spectral components and disappearance of magnetic hyperfine splitting at certain values of the parameters V, K and T. As a result, the relaxation component of the spectra is formed. Lowering the measurement temperature makes it possible to freeze fluctuations in the magnetic moments of particles, therefore the Mössbauer spectra measured at 900 K show two resolved magnetic sextets, which correspond to Fe nuclei with different magnetic neighborhoods. The broadened sextet components of the spectra of the

Table 1

Parameters of the Mössbauer spectra of the $CuFe_2O_4/rGO$ composite at 90 K

Site	Is, mm/s	Qs, mm/s	H, kOe	S, %	G, mm/s
A	0.39	-0.02	519	47.0	0.49
B	0.27	-0.01	489	53.0	0.44

$CuFe_2O_4/rGO$ sample at room temperature correspond to an intermediate stage between the magnetically ordered (MO) and superparamagnetic (SP) states of oxide particles [11]. The values of the isomer shift (IS), quadrupole splitting (QS), hyperfine magnetic field (B), Lorentizan line width (w), and relative integral intensity (I) were obtained using the fitting procedure (Table 1). $CuFe_2O_4$ is a partially inverse spinel – Cu^{2+} and Fe^{3+} ions are located in crystalline and magnetic nonequivalent tetrahedral and octahedral sites (A and B, respectively) [12]. The cation distribution can be described as $(Cu_xFe_{1-x})_A[Cu_{1-x}Fe_{1+x}]_BO_4$, where x is the inversion parameter ($x = 0$ and $x = 1$ denote the inverse and normal, respectively). The identification of the sublattice for $CuFe_2O_4/rGO$ sample at 90 K was based on the relatively higher values of the hyperfine magnetic field and isomer shift for ^{57}Fe nuclei in the octahedral site (B-sublattice) [13].

The degree of inversion (the fraction of tetrahedrally coordinated Fe^{3+} cations) is determined by the ratio of the relative intensities of the corresponding components S_A and S_B of the spectra: $\frac{S_A}{S_B} = \frac{f_A}{f_B} \times \frac{2-x}{x}$, where f_A and f_B are the values of the recoilless fractions for the tetrahedrally and octahedrally coordinated Fe nuclei, $f_B/f_A = 0.94 \pm 0.01$ [14].

The ratio between the relative intensity of the sub-spectra corresponding to A- and B-sublattices is 0.89, so the inverse degree is close to 1. The estimated cation distribution for the spinel phase of $CuFe_2O_4/rGO$ composite materials is $(Fe)_A[CuFe]_BO_4$. The conditions of MO/SP transition depend on the average particle size, temperature and magnetocrystalline anisotropy. The value of magnetocrystalline anisotropy for $CuFe_2O_4$ is about $0.6 \cdot 10^4$ J·m^{-3} [15], therefore, particles with an average size of less than 8 nm will retain superparamagnetic properties at 90 K.

The nitrogen adsorption-desorption isotherms for $CuFe_2O_4/rGO$ composites, as well as for pure rGO and $CuFe_2O_4$, are shown in Fig. 3. According to the IUPAC classification, the rGO sample, exhibited type IV isotherms, indicates the presence of both micro- and mesopores. The H4 hysteresis loop is clearly associated with a narrow slit-like pore [16]. The calculated pore size distribution (see inset in Fig. 3, a) shows a spectrum of pore diameters with maxima in the microporous region at about 1.4 nm. The N_2 adsorption/desorption isotherm for hydrothermally obtained $CuFe_2O_4$ also belongs to type IV, but the hysteresis loop arising in the range of relative pressures $0.6 < p/p_0 < 1$ is associated only with the capillary condensation in mesopores.
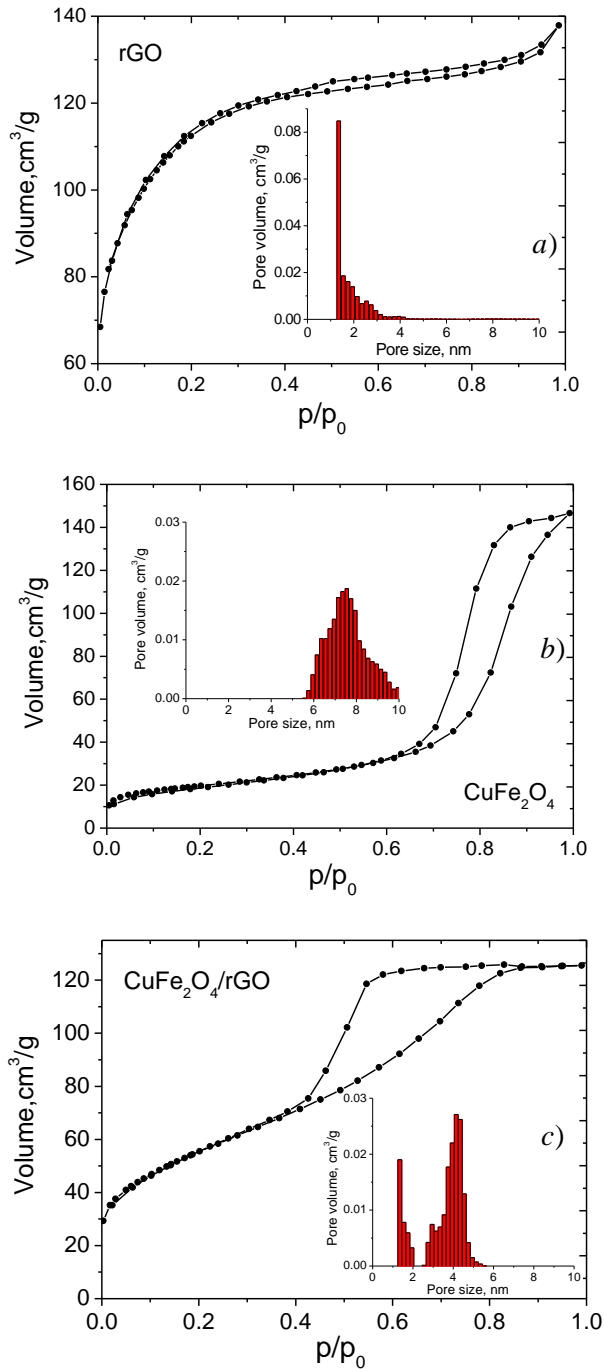
Fig.3. Pore size distribution for as-synthesized $CuFe_2O_4$ and $CuFe_2O_4 / rGO$ samples.

The pore size distribution of the spinel sample (inset in Fig. 3,b) reveals a character close to normal, with an average pore diameter of about 7.8 nm, which is consistent with XRD data. The $CuFe_2O_4 / rGO$ sample exhibits the nitrogen adsorption character that is different from both pure components. The shift of the wide H2 type hysteresis loop to $p/p_0 \approx 0.4$ of the type IV isotherm indicates the predominance of the pore size in the mesoporous region. The sharp step of pore emptying at the lower limit of the capillary condensation hysteresis is probably the result of the presence of a bottle-neck or mesoporous structure with vaguely defined pore size and shape [17]. The $CuFe_2O_4 / rGO$ composite exhibits a

correspondingly higher dispersion of spinel nanoparticles compared to $CuFe_2O_4$, resulting in improved porosity and increased surface area. The BET specific surface areas of pure rGO and $CuFe_2O_4$ were 414 m^2/g and 72 m^2/g, respectively. The specific surface area of the $CuFe_2O_4 / rGO$ composites was about 193 m^2/g, which indicates that rGO successfully prevents the aggregation of spinel particles directly at the nucleation stage.

It can be assumed that the composite material is formed by clusters of spinel phase particles covered with packages of stacking graphene layers separated by porous rGO. The bimodal pore size distribution (inset in Fig. 3,c) can be associated with the micropore structure of the rGO component and the mesopore structure of the $CuFe_2O_4 / rGO$ combined particles, respectively.

Electrical conductivity σ for both $CuFe_2O_4$ and $CuFe_2O_4 / rGO$ samples increases with increasing frequency in the temperature range of 25 - 200 °C (Fig. 4, a-b). The temperature dependences of σ_{ac} values are more complex (Fig. 4, c-d). Electrical conductivity for both samples increases to 125 °C with the next despite. Negative $d\sigma/dT$ values at the temperature range of 150-200 °C are caused by scattering of charge carriers on grain boundaries. Interparticle hopping transport of charge carriers is the dominating mechanism of electrical conductivity of spinel nanopowders [18].

In the complex impedance spectra of both samples, a decrease in the real and imaginary parts of electrical resistance is observed in the temperature range of 25 - 125°C. The Nyquist plots of the $CuFe_2O_4$ sample are characterized by semicircular arcs at 25 - 50 °C (correspond to a parallel combination of resistance and capacitance) with the evolution of changes at the temperature increasing and additional small semicircles forming at high frequencies (Fig. 5, a).

The Nyquist plots of the $CuFe_2O_4 / rGO$ composite material (Fig. 5, b) have a linear section in the high-frequency region, which turns into a semicircle with increasing temperature. Analysis of impedance spectra and selection of an equivalent electrical circuit (EEC) provide information on the mechanisms of charge transfer. The optimal approximation of the experimental data of the complex impedance was achieved using the EEC shown in Fig. 5, c. A similar approach was used by [19] to describe the dielectric behavior of nanocrystalline spinel $NiFe_2O_4$.

The best fitting results for $CuFe_2O_4$ were obtained with the R_g-(R_H-CPE) scheme, but for rGO-contained material, there is an additional series (R_L-CPE) chain (Fig. 5, c).

A constant phase element (CPE) is described as: $Z_{CPE} = [Q(j\omega)^n]^{-1}$, where Q is a frequency independent parameter and $0 < n < 1$ (n = 1 for pure capacitors, n = 0 for pure resistance and n = 0.5 for Warburg element). Constant phase elements were used instead of pure capacitors to take into account the high morphological and electrical inhomogeneity of the sample. These parameters were calculated by analyzing Nyquist plots using a nonlinear least squares fit procedure with ZView software. The evolution of fitting parameters with increasing temperature is shown in Fig. 6, a-b.
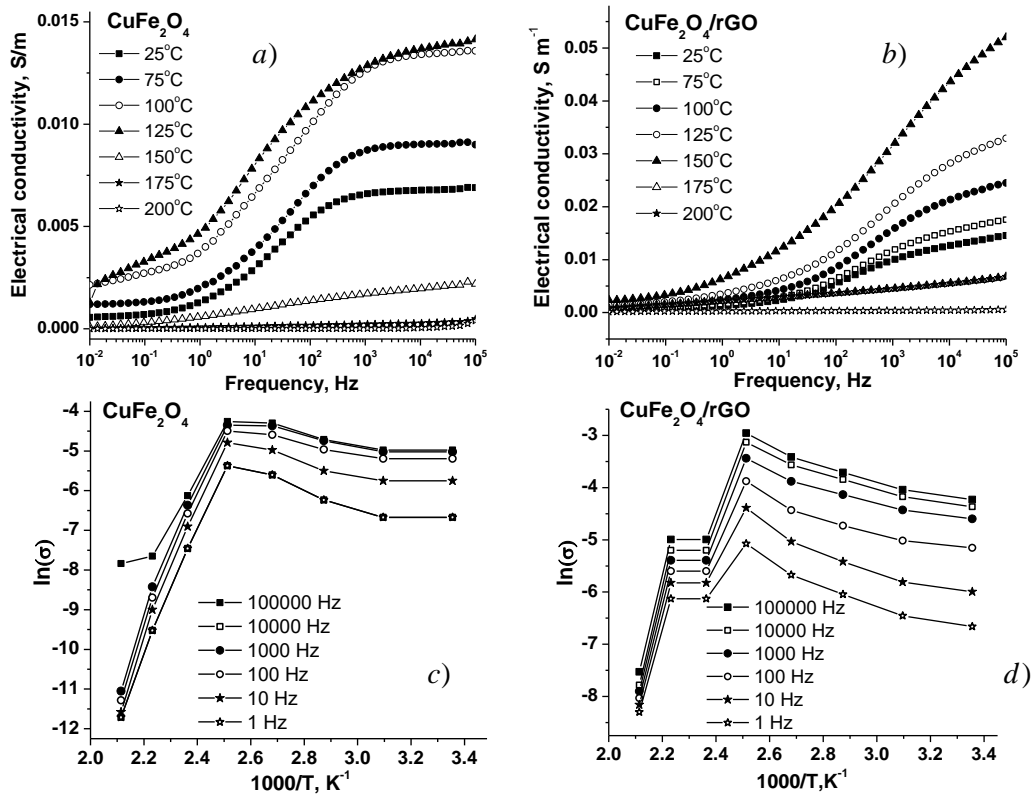
Fig. 4. Frequency dependences of the real part of electrical conductivity of (a) $CuFe_2O_4$ and (b) $CuFe_2O_4/rGO$ samples; as well as (c, d) corresponding Arrenius plots ($\ln(\sigma_{ac})$ versus 1000/T) for selected frequencies
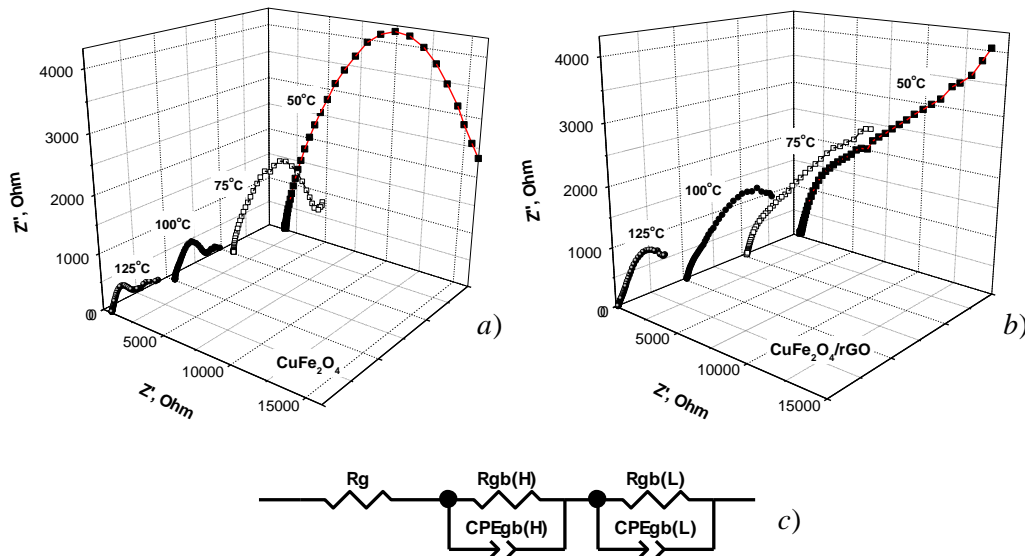

Fig. 5. Nyquist plots of (a) $CuFe_2O_4$ and (b) $CuFe_2O_4 / rGO$ samples at temperatures of 50, 75, 100 and 125 °C, as well as (c) the equivalent electrical circuit used for its fitting.

It can be assumed that R_g corresponds to the inner resistance of particles, when R_H and R_H, according to the EEC, are associated with grain boundaries (Fig. 7, a-b). The R_L parameter can be attributed to the charge transfer resistance between rGO particles (Fig. 7, b).

The correspondingly lower values of R_g parameters for the $CuFe_2O_4/rGO$ sample as compared to pure spinel are caused by the better interparticle ohmic contact for the correspondingly smaller average size of the oxide particles. At the same time, the lower rate of decrease in R_H parameters of the composite material can be explained by the higher concentration of defects as the centers of scattering of charge carriers in near-surface regions of spinel particles.
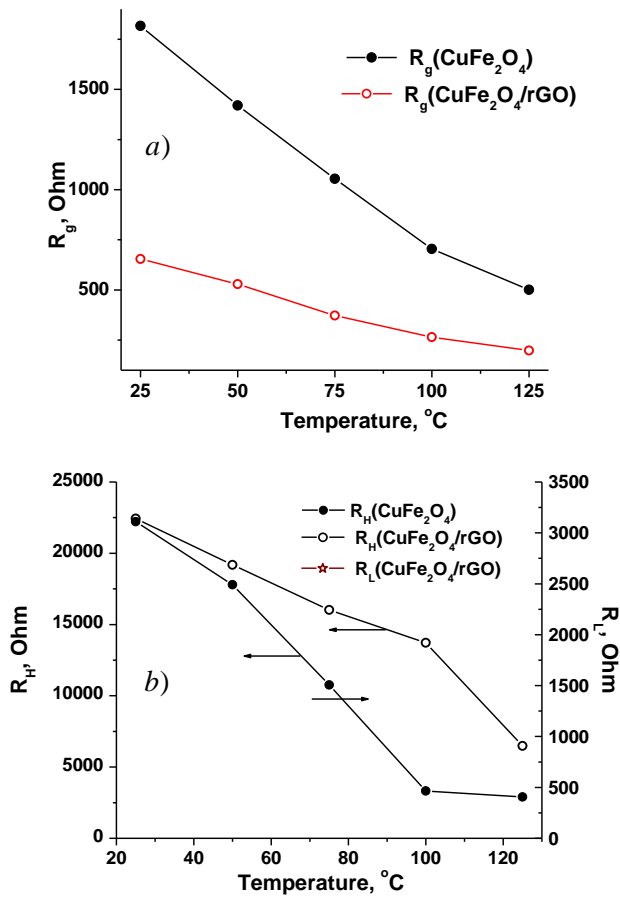
Fig. 6. Temperature dependences of the fitting parameters of the impedance spectra of $CuFe_2O_4$ and $CuFe_2O_4$ / rGO samples.

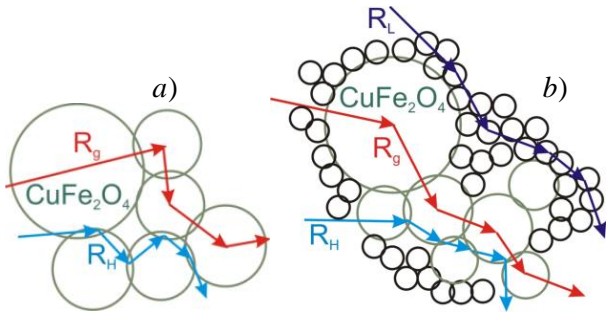**Fig. 7.** Models of charge transfer mechanisms for $CuFe_2O_4$ and $CuFe_2O_4$ / rGO materials.

Obviously, this is a strong dependence of investigated porous materials on pressure conditions, but understanding of the charge transfer mechanism makes it possible to control the electrophysical properties of materials.

The values of the resistance R_g, as well as the resistances R_H and R_L, were used to calculate the AC conductivity of the grain (σ_g) and the grain boundary (σ_H, σ_L), respectively.

The increase in AC conductivity with temperature is caused by an increase in the thermally activated hopping mobility of charge carriers. The value of the activation energy of charge carriers hopping was calculated using

the Arrhenius equation $\sigma = \dfrac{\sigma_0}{T} \exp\left[-\dfrac{E_a}{kT} \right]$, where σ_0 is the pre-exponential factor, E_a is the activation energy, and k is the Boltzmann constant [18]. The Arrhenius dependences of $\ln(\sigma T)$ vs. T^{-1} were plotted and linearized for the temperature range of 25-125 °C (Fig. 8, a-b).

The activation energies of charge carriers hopping between oxide grains for pure $CuFe_2O_4$ are correspondingly lower than those for spinel grains in the $CuFe_2O_4$ / rGO sample (Fig. 8, a), which is due to the larger particle size. The activation energies of hopping conductivity along grain boundaries for $CuFe_2O_4$ are more than two times higher than the characteristics of the $CuFe_2O_4$ / rGO powder due to the charge transport optimization in mixed two-phase composite particles. The correspondingly large value of E_a for the electrical conductivity of the rGO component can be explained by both low density and capacitive effects (Fig. 8, b).
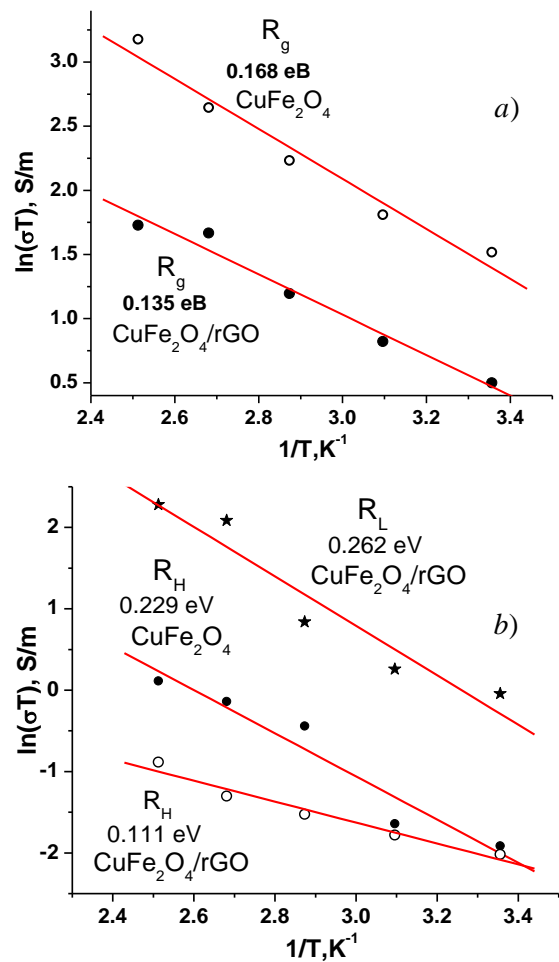

Fig. 8. Arrhenius plots for $CuFe_2O_4$ and $CuFe_2O_4$ / rGO samples (solid lines are the best fit).

Conclusion

A comparative analysis of the structural and electrical conductivity properties of the hydrothermally synthesized nanocrystalline $CuFe_2O_4$ spinel and $CuFe_2O_4$ / rGO composite (the mass ratio of spinel and graphene components is about 1:1) has been carried out.

V.O. Kotsyubynsky, V.M. Boychuk, R.I. Zapukhlyak, M.A. Hodlevskyi, I.M. Budzulyak, A.I. Kachmar, etc.

A pure $CuFe_2O_4$ material with an average size of ferrite powder of about 14.5 nm has been obtained, when the spinel phase of the $CuFe_2O_4$/rGO composite consists of particles with an average diameter of less than 8 nm. The rGO component has successfully prevented the aggregation of spinel particles at the nucleation stage during joint synthesis of the spinel phase and graphene oxide reduction. As a result, the composite material consists of a spinel particle covered with rGO clusters separated by porous rGO.

The specific surface areas of rGO and $CuFe_2O_4$ were 414 m^2/g and 72 m^2/g, respectively, while for the $CuFe_2O_4$ / rGO composite, $S_{BET} = 193$ m^2/g with a bimodal pore size distribution corresponding to micropores rGO and mesopores $CuFe_2O_4$ / rGO combined particles. Analysis of impedance spectra and the choice of an equivalent electrical circuit provide information on the charge transfer mechanisms and trace the electrical conductivity of the grain and grain boundaries. An increase in the activation energy of charge carrier hopping transport into oxide grains (0.135 eV and 0.168 eV for $CuFe_2O_4$ and $CuFe_2O_4$ / rGO materials, respectively) is the result of a correspondingly smaller size of particles of the oxide phase in the composite material. At the same time, the grain boundary hopping $CuFe_2O_4$/ rGO composite is energetically favorable (0.111 eV and 0.229 eV for $CuFe_2O_4$ and $CuFe_2O_4$ / rGO materials, respectively). Thus, the results obtained suggest that the $CuFe_2O_4$ / rGO composites are promising candidates as electrode materials for hybrid supercapacitors.

KotsyubynskyV.O. – Professor, Doctor of Physical and Mathematical Sciences;
Boychuk V.M. – Professor, Doctor of Physical and Mathematical Sciences;
Zapukhlyak R.I. – Assistant Professor, Ph.D;
Hodlevskyi M.A. - Ph.D student;
Budzulyak I.M. – Professor, Doctor of Physical and Mathematical Sciences;
Kachmar A.I. - Ph.D.
Hodlevska M.A. – Ph.D student
Turovska L.V. - Assistant Professor, Ph.D.

[1] Malaie, M. R. Ganjali, Journal of Energy Storage 102097 (2020); https://doi.org/10.1016/j.est.2020.102097.
[2] J.S. Sagu, K.G.U. Wijayantha, A.A. Tahir, Electrochimica Acta 246, 870 (2017); https://doi.org/10.1016/j.electacta.2017.06.110.
[3] S.L. Kuo, J. F. Lee, N.L. Wu, Journal of the Electrochemical Society 154(1), A34 (2006).
[4] P. Bhojane, A. Sharma, M. Pusty, Y. Kumar, S. Sen, P. Shirage, Journal of nanoscience and nanotechnology 17(2), 1387 (2017); https://doi.org/10.1166/jnn.2017.12666.
[5] V. Boychuk, V. Kotsyubynsky, B. Rachiy, Kh. Bandura, A. Hrubiak, S. Fedorchenko, Materials Today: Proceedings 6(2), 106 (2019); https://doi.org/10.1016/j.matpr. 2018.10.082.
[6] V. Kotsyubynsky, R. Zapukhlyak, V. Boychuk, M. Hodlevska, B. Rachiy, I. Yaremiy, A. Kachmar, M. Hodlevsky, Applied Nanoscience 1-8 (2021); https://doi.org/10.1007/s13204-021-01773-z.
[7] V.O. Kotsyubynsky, V.M. Boychuk, B.I. Mudzuliak, B.I. Rachiy, R.I. Zapukhlyak, M.A. Hodlevska, et all., Physics and Chemistry of Solid State, 22(1), 31 (2021); https://doi.org/10.15330/pcss.22.1.31-38.
[8] S. Pei, H. M. Cheng, Carbon 50(9), 3210 (2012); https://doi.org/10.1016/j.carbon.2011.11.010.
[9] V. Kotsyubynsky, B. Ostafiychuk, V. Moklyak, A. Hrubiak, Solid State Phenomena 230, 120 (2015); https://doi.org/10.4028/www.scientific.net/SSP.230.120.
[10] O. Petracic, Superlattices and Microstructures 47(5), 569 (2010); https://doi.org/10.1016/j.spmi.2010.01.009.
[11] G.F Goya, H.R. Rechenberg, Nanostructured Materials 10(6), 1001 (1998); https://doi.org/10.1016/S0965-9773(98)00133-0.
[12] J.J. Z.iang, G.F. Goya, H.R. Rechenberg, Journal of Physics: Condensed Matter 11(20), 4063 (1999).
[13] R.K., Selvan, C.O., Augustin, V. Šepelák, L.J. Berchmans, C.bSanjeeviraja, & A. Gedanken, Materials Chemistry and Physics 112(2), 373 (2008).
[14] S.Da Dalt, A.S. Takimi, T.M. Volkmer, V.C. Sousa, C.P. Bergma, Powder Technology 210(2), 103 (2011); https://doi.org/10.1016/j.powtec.2011.03.001.
[15] I. Nedkov, R.E. Vanderberghe, G. Vissokov, T. Merodiiska, S. Kolev, K. Krezhov, Physica Status Solidi 201(5), 1001 (2004); https://doi.org/10.1002/pssa.200306788.
[16] M. El-Shahat, M. Mochtar, M.M. Rashad, & M.A. Mousa, Journal of Solid State Electrochemistry 25(3), 803 (2021); https://doi.org/10.1007/s10008-020-04837-2.
[17] S.V. Moghaddam, M. Rezaei, F. Meshkani, R. Daroughegi, International journal of hydrogen energy 43(41), 19038 (2018); https://doi.org/10.1016/j.ijhydene.2018.08.163.
[18] B.K. Ostafiychuk, L.S. Kaykan, J.S. Mazurenko, B.Y. Deputat, S.V. Koren, Journal of Nano-and Electronic Physics 9(5), (2017); https://doi.org/10.21272/jnep.9(5).05018.
[19] N. Ponpandian, P. Balaya, A. Narayanasamy, Journal of Physics: Condensed Matter 14(12), 3221 (2002); https://doi.org/10.1088/0953-8984/14/12/311.

В.О. Коцюбинський[1], В.М. Бойчук[1], Р.І. Запухляк[1], М.А. Годлевський[1], І.М. Будзуляк[1], А.І. Качмар[2], М.А Годлевська[1], Л.В. Туровська[3]

Електрофізичні та морфологічні властивості синтезованого гідротермічним методом CuFe$_2$O$_4$ та CuFe$_2$O$_4$ / відновленого композиту оксиду графену

[1]*Прикарпатський національний університет імені Василя Стефаника”, Івано-Франківськ, Україна, kotsuybynsky@gmail.com*
[2]*Познанський технічний університет, Познань, Польша andrij.nj@gmail.com*
[3]*Івано-Франківський національний медичний університет, Івано-Франківськ, Україна, lturovska@gmail.com*

Метою роботи є порівняння структурних, морфологічних та електрофізичних властивостей композиту CuFe$_2$O$_4$ та композиту CuFe$_2$O$_4$ / відновленого оксиду графену, отриманих методом гідротермального синтезу. Відповідно до результатів рентгеноструктурного аналізу та месбауерівської спектроскопії показано, що сумісний синтез кубічного фериту міді та відновлення оксиду графену призводять до зменшення часток фериту з 14 до 8 нм в порівняння з матеріалом без вуглецевої компоненти, отриманого аналогічним способом. Відповідно до розробленої на основі результатів досліджень методом імпедансної спектроскопії, композитний матеріал CuFe$_2$O$_4$ / відновлений оксид графену представляє собою систему, що складається з контактуючих оксидних частинок зі структурою шпінелі, покритих кластерами відновленого оксиду графену і розділених пористим шаром цього ж матеріалу. Для CuFe$_2$O$_4$ / rGO показано домінування механізмів стрибкоподібного переносу заряду та розраховано енергії активації електропровідності.

Ключові слова: ферит міді, відновлений оксид графену, мессбауерівська спектроскопія, електропровідність.